The $Zb\bar{b}$ Couplings at Future e^+e^- Colliders

Stefania Gori,[a,1] **Jiayin Gu,**[b,2] **Lian-Tao Wang** [c,d,3]

[a] *Perimeter Institute for Theoretical Physics, 31 Caroline St. N, Waterloo, Ontario, Canada N2L 2Y5.*

[b] *Center for Future High Energy Physics, Institute of High Energy Physics, Chinese Academy of Sciences, Beijing 100049, China.*

[c] *Enrico Fermi Institute, University of Chicago, Chicago, IL 60637.*

[d] *Kavli Institute for Cosmological Physics, University of Chicago, Chicago, IL 60637.*

Abstract

Many new physics models predict sizable modifications to the SM $Zb\bar{b}$ couplings, while the corresponding measurements at LEP and SLC exhibit some discrepancy with the SM predictions. After updating the current results on the $Zb\bar{b}$ coupling constraints from global fits, we list the observables that are most important for improving the $Zb\bar{b}$ coupling constraints and estimate the expected precision reach of three proposed future e^+e^- colliders, CEPC, ILC and FCC-ee. We consider both the case that the results are SM-like and the one that the $Zb\bar{b}$ couplings deviate significantly from the SM predictions. We show that, if we assume the value of the $Zb\bar{b}$ couplings to be within 68% CL of the current measurements, any one of the three colliders will be able to rule out the SM with more than 99.9999% CL (5σ). We study the implications of the improved $Zb\bar{b}$ coupling constraints on new physics models, and point out their complementarity with the constraints from the direct search of new physics particles at the LHC, as well as with Higgs precision measurements. Our results provide a further motivation for the construction of future e^+e^- colliders.

[1] sgori@perimeterinstitute.ca

[2] gujy@ihep.ac.cn

[3] liantaow@uchicago.edu

Contents

1 Introduction **3**

2 Current constraints on the $Zb\bar{b}$ couplings **5**

3 $Zb\bar{b}$ coupling constraints from future e^+e^- colliders **9**

3.1 Precision of the EWPOs at future e^+e^- colliders 10

3.2 SM-like measurements and constraints on NP 13

3.3 Discovering NP through $A_{FB}^{0,b}$ ($\mathcal{A}_b$) 14

4 Implication on NP models **15**

4.1 Two Higgs doublet models 17

4.2 Composite Higgs models 19

4.3 The Beautiful Mirror Model 21

5 Conclusion **24**

A Theoretical uncertainties **25**

1 Introduction

The LHC has just started to run at an unprecedented center-of-mass energy, 13 TeV, and will be able to probe new physics (NP) at higher energies. At the same time, precision measurements of electroweak physics at future e^+e^- machines will also offer powerful probes of Beyond the Standard Model (BSM) physics.

The next lepton collider may not be too distant in the future from us. Several compelling plans exist, including the International Linear Collider (ILC) [1], FCC-ee, formerly known as TLEP [2], and the Circular Electron-Position Collider (CEPC) [3]. With the discovery of the Higgs boson, the primary goal of such future e^+e^- colliders will be to produce a large sample of Higgs boson events at around ~ 250 GeV to precisely measure the Higgs boson's properties, acting as a "Higgs factory". On the other hand, such e^+e^- colliders could also collect large amount of data around the Z-pole, producing several orders of magnitude more Z-bosons than what was produced at LEP. The large amount of Z-pole data would greatly improve the measurement of the several electroweak precision observables (EWPOs), which could provide strong constraints on NP.

Several studies on the measurement of EWPOs at future e^+e^- colliders have been performed [4–7], mainly focusing on the oblique corrections parameterized by the Peskin-Takeuchi parameters S and T [8]. NP could also have sizable non-universal corrections. The corrections to the $Zb\bar{b}$ vertex is particularly interesting, and quite generic in NP models. For example, being the left-handed top and bottom quarks in the same electroweak (EW) doublet, new physics that couples to the top quark usually also affects the $Zb\bar{b}$ couplings [9]. Composite Higgs models with light top partners usually predict a large correction to the $Zb_L\bar{b}_L$ coupling, unless it is protected by some symmetry analogous to the custodial symmetry that protects the weak isospin [10]. Additionally, heavy Higgs bosons typically couple more strongly to the third generation quarks and modify the $Zb\bar{b}$ coupling through loops [11].

The story is even more interesting on the experimental side. At LEP, the left and right handed $Zb\bar{b}$ couplings are mainly determined by two measurements at the Z-pole: R_b^0, the ratio of the $Z \to b\bar{b}$ partial width to the inclusive hadronic width, and $A_{\rm FB}^{0,b}$, the forward-backward asymmetry of the bottom quark. The measured value of R_b^0 agrees with the most recent two-loop calculation of its SM prediction within $1\,\sigma$ [12–14]. $A_{\rm FB}^{0,b}$, instead, exhibits a long-standing discrepancy with the SM prediction with a significance at around $2.5\,\sigma$ [12, 14]. In addition, SLD directly measured the bottom quark asymmetry

	measured value	SM prediction
R_b^0	0.21629 ± 0.00066	0.21578 ± 0.00011
$A_{\rm FB}^{0,b}$	0.0992 ± 0.0016	0.1032 ± 0.0004
$\mathcal{A}_b$	0.923 ± 0.020	0.93463 ± 0.00004

Table 1: The measured values and SM predictions of R_b^0, $A_{\rm FB}^{0,b}$ and $\mathcal{A}_b$ according to the most recent result from the Gfitter group [14].

with longitudinal beam polarizations, $\mathcal{A}_b$, which is consistent with the SM prediction within $1\,\sigma$ but slightly prefers a shift in the same direction as the LEP $A_{\rm FB}^{0,b}$ measurement does. The measured values and SM predictions of R_b^0, $A_{\rm FB}^{0,b}$ and $\mathcal{A}_b$ are summarized in Table 1[4]. To obtain the desired modification for $A_{\rm FB}^{0,b}$ without violating the experimental constraint on R_b^0 and $\mathcal{A}_b$, a simultaneous modification of both the $Zb_L\bar{b}_L$ and $Zb_R\bar{b}_R$ couplings is required. To obtain the best estimation for the preferred values of the $Zb_L\bar{b}_L$ and $Zb_R\bar{b}_R$ couplings, a global fit to all precision data has to be performed (see e.g. [16,17], for earlier studies).

A future e^+e^- collider offers great opportunities for further studies on the $Zb\bar{b}$ couplings. With the huge improvement on statistics at Z-pole, it will surely have the potential to resolve the $A_{\rm FB}^{0,b}$ discrepancy at LEP. If the result agrees with the SM predictions, a e^+e^- collider can provide very strong constraint on NP models; if the LEP $A_{\rm FB}^{0,b}$ discrepancy does come from NP, a e^+e^- collider will have the potential to rule out the SM with enough significance, therefore providing strong indirect evidence for physics beyond the SM. In either case, the results would greatly improve our understanding of fundamental particle physics. In this paper, we perform a study of the constraints on non-universal modifications of the $Zb\bar{b}$ couplings from prospective precisions at future e^+e^- colliders, which, to our best knowledge, is the first study of such kind.

The rest of this paper is organized as follows. In Section 2, we review the current constraints on the $Zb\bar{b}$ couplings and discuss the importance of including the strong coupling constant in the global fit. In Section 3, we compare the precision reaches of the three proposed e^+e^- colliders and outline the most important measurements needed for improving the $Zb\bar{b}$ coupling constraints. We then perform a model independent analysis to constrain the effective Lagrangian responsible of the modifications of the $Zb\bar{b}$ vertex, in both the case that the results are SM-like and the one that NP causes a significant

[4] Ref. [15] quotes a value of 0.00015 as the theoretical uncertainty for the SM prediction for R_b^0. Either way, the current theoretical uncertainty of R_b^0 is too small to have an impact on the current precision data.

deviation in the bottom asymmetries. In Section 4, we interpret these constraints on specific NP scenarios including two Higgs doublet models (2HDMs), composite Higgs models and the Beautiful Mirror Model. We will compare these constraints to the direct reach of the NP particles at the LHC, as well as to the constraints from oblique parameters and Higgs precision measurements. In Section 5, we present our conclusions. Finally, in Appendix A, we discuss our treatment of theory uncertainties.

2 Current constraints on the $Zb\bar{b}$ couplings

In this section we present the constraints on the $Zb\bar{b}$ couplings from the global fit of the current precision electroweak data. We follow closely the fit procedure of the Gfitter group [14, 18][5], with the Z-pole data from LEP, SLD [12] along with the measurements of the W, top and Higgs masses [24–27] and the hadronic contribution to the running fine structure constant [28][6]. In particular, our procedure uses the input parameters and the electroweak and QCD corrections to the electroweak observables of the latest GFitter analysis [14], even though it does not make use of the GFitter public code.

There are, in fact, a few important differences between our procedure and the one of the Gfitter group. First, we include the world average of the strong coupling constant $\alpha_S(M_Z^2)$ [24, 30] (denoted as $\alpha_S(M_Z^2)_{\rm avg.}$) as a constraint in the fit[7]. Later in this section, we will show that the inclusion of $\alpha_S(M_Z^2)_{\rm avg.}$ has a moderate, but non-negligible, impact on the constraints of the $Zb\bar{b}$ couplings[8]. Second, the observable $\sin^2\theta^l_{\rm eff}(Q_{\rm FB})$ is not included in our fit. $\sin^2\theta^l_{\rm eff}(Q_{\rm FB})$ is a direct measurement of the leptonic effective weak mixing angle at LEP, using the charge forward backward asymmetry. Its measurement has a strong model dependence and the LEP result explicitly assumes the SM, therefore it is difficult to interpret this measurement in the presence of vertex corrections. In practice, this observable is not precisely measured and has a small impact in the global fit. To summarize, the SM free parameters considered in our fit are $M_H\,,\ M_Z\,, m_{\rm top}\,, \Delta\alpha^{(5)}_{\rm had}$ and $\alpha_S(M_Z^2)$. The additional observables included in our fit are Γ_Z, $\sigma^0_{\rm had}$, R^0_l, $A^{0,l}_{\rm FB}$, $\mathcal{A}_l$, $\mathcal{A}_c$,

[5]For a global fit in the context of the Standard Model effective field theory, see e.g. [19–23].

[6]It should be noted that there also exist non-trivial bounds on the $Zb\bar{b}$ couplings from hadron colliders, as pointed out in *e.g.* Ref. [29], although the precision can not compete with the one obtained from lepton colliders.

[7]The value we use is $\Delta\alpha^{(5)}_{\rm had} = (2757 \pm 10) \times 10^{-5}$.

[8]Ref. [17], [31] and [24] included $\alpha_S(M_Z^2)_{\rm avg.}$ but did not comment on its impact on the $Zb\bar{b}$ couplings.

$\mathcal{A}_b$, $A_{\rm FB}^{0,c}$, $A_{\rm FB}^{0,b}$, R_c^0, R_b^0, M_W and Γ_W.

The coupling of the Z to left and right handed bottoms, denoted by g_{Lb} and g_{Rb}, are given in the following interaction term,

$$\mathcal{L} \supset \frac{g}{c_W} Z_\mu (g_{Lb} \bar{b}_L \gamma^\mu b_L + g_{Rb} \bar{b}_R \gamma^\mu b_R) \,, \tag{2.1}$$

where $c_W \equiv \cos\theta_W$, with θ_W the weak mixing angle, and g is the $SU(2)$ gauge coupling. Through out this paper we shall use δg_{Lb} and δg_{Rb} to parameterize the modification of the $Zb\bar{b}$ couplings, defined as

$$g_{Lb} = g_{Lb}^{\rm SM} + \delta g_{Lb} \,, \quad g_{Rb} = g_{Rb}^{\rm SM} + \delta g_{Rb} \,, \tag{2.2}$$

where $g_{Lb}^{\rm SM}$ and $g_{Rb}^{\rm SM}$ are the SM predictions for g_{Lb} and g_{Rb}, which at the tree level are given by

$$g_{Lb}^{\rm SM,0} = -1/2 + s_W^2/3 \simeq -0.42 \,, \quad g_{Rb}^{\rm SM,0} = s_W^2/3 \simeq 0.077 \,. \tag{2.3}$$

At the tree level, R_b^0, $\mathcal{A}_b$ and $A_{\rm FB}^{0,b}$ at Z-pole can be written as

$$R_b^0 = \frac{g_{Lb}^2 + g_{Rb}^2}{\sum\limits_q (g_{Lq}^2 + g_{Rq}^2)} \,, \tag{2.4}$$

where $\sum\limits_q$ denotes a sum over all quarks except the top quark, and

$$\mathcal{A}_b = \frac{g_{Lb}^2 - g_{Rb}^2}{g_{Lb}^2 + g_{Rb}^2} \,, \quad A_{\rm FB}^{0,b} = \frac{3}{4} \mathcal{A}_e \mathcal{A}_b = \frac{3}{4} \frac{g_{Le}^2 - g_{Re}^2}{g_{Le}^2 + g_{Re}^2} \frac{g_{Lb}^2 - g_{Rb}^2}{g_{Lb}^2 + g_{Rb}^2} \,. \tag{2.5}$$

These expressions will be modified once loop corrections are included.

It should be pointed out that the measurements at Z-pole alone could not determine the signs of g_{Lb} and g_{Rb}. The off-peak measurements can resolve the sign ambiguities due to interference of the Z diagram with the s-channel photon diagram. However, as pointed out in Ref. [32], the LEP data at scales different from m_Z are limited in statistics and could definitely resolve the sign of g_{Lb}, but not the one of g_{Rb}. Nevertheless, NP theories able to flip the sign of g_{Rb} are typically in tension with other EW precision data such as the constraints on S and T parameters [16, 32]. Future lepton colliders will collect a large amount of data at higher scales, which should completely resolve this ambiguity[9].

[9]As an example, the value of $A_{\rm FB}^{0,b}$ at around 240 GeV is changed by ~ 0.2 if the sign of g_{Rb} is flipped with respect to the SM prediction. On the other hand, the proposed CEPC run at ~ 240 GeV would collect 5 ab^{-1} of data over ten years with two detectors [3], resulting in a statistical uncertainty of ~ 0.0003 for $A_{\rm FB}^{0,b}$, which is sufficient for resolving the sign of g_{Rb} as long as enough events are left after the event selection and the systematics are under control.

In this paper we do not consider the possibility that g_{Rb} has the opposite sign of its SM prediction.

The potential NP that modifies the $Zb\bar{b}$ couplings can also change other EW observables. To capture the most relevant corrections without relying too much on the model assumptions, we will consider NP scenarios that contribute to the oblique parameters S and T along with the modified $Zb\bar{b}$ couplings. Therefore, our minimal model assumption is SM together with S, T, δg_{Lb} and δg_{Rb} treated as free parameters. For later convenience we will denote it as (SM+$S, T, \delta g_{Lb}, \delta g_{Rb}$).

With the model assumptions and fit procedure described above, we obtain the constraints on δg_{Lb} and δg_{Rb}, shown in Fig. 1. The blue (orange) region corresponds to a confidence level (CL) smaller than 68% (95%), while the green dot is the SM prediction ($\delta g_{Lb} = \delta g_{Rb} = 0$). In addition, in the left plot we show the individual constraints from R_b^0 (red) and the combination of $\mathcal{A}_b$ and $A_{\rm FB}^{0,b}$ (cyan), for which the parameters other than δg_{Lb} and δg_{Rb} are set to the best-fit values. This verifies that R_b^0 and $A_{\rm FB}^{0,b}(\mathcal{A}_b)$ are the most relevant measurements for constraining the $Zb\bar{b}$ couplings. Given that δg_{Lb} and δg_{Rb} are relatively small, the change in R_b^0, $A_{\rm FB}^{0,b}$ and $\mathcal{A}_b$ can be expanded in terms of δg_{Lb} and δg_{Rb}. Keeping the first order, while fixing the other parameters to the best-fit values, we obtain

$$\begin{aligned} \delta R_b^0 &\approx -0.78\,\delta g_{Lb} + 0.14\,\delta g_{Rb}\,, \\ \delta A_{\rm FB}^{0,b} &\approx -0.034\,\delta g_{Lb} - 0.18\,\delta g_{Rb} \approx 0.11 \times \delta\mathcal{A}_b\,. \end{aligned} \tag{2.6}$$

As shown in Table 1, the current experimental (1σ) uncertainties are 0.00066 for R_b^0 and 0.0016 (0.020) for $A_{\rm FB}^{0,b}$ ($\mathcal{A}_b$). These numbers together with Eq. (2.6) provide a good analytical understanding of the $Zb\bar{b}$ coupling constraints. First, R_b^0 is more constraining than $A_{\rm FB}^{0,b}(\mathcal{A}_b)$ and leads to a large positive correlation between δg_{Lb} and δg_{Rb}. Second, R_b^0 is numerically more sensitive to δg_{Lb} while $A_{\rm FB}^{0,b}(\mathcal{A}_b)$ is more sensitive to δg_{Rb}.

As mentioned previously, in our fit we have included $\alpha_S(M_Z^2)_{\rm avg.}$ (world average) as a constraint in the global fit. $\alpha_S(M_Z^2)_{\rm avg.}$ includes several different measurements, but is dominated by the lattice calculation [24, 30]. More explicitly, to avoid double counting, we use the PDG world average excluding electroweak precision test (EWPT) results [24], which is

$$\alpha_S(M_Z^2)_{\rm avg.} = 0.1185 \pm 0.0005 \quad \text{(world average w/o EWPT result)}\,. \tag{2.7}$$

The Gfitter group [14, 18] does not include this constraint in the fit, since the global fit for the SM and also for the oblique parameters S and T is not sensitive to $\alpha_S(M_Z^2)_{\rm avg.}$.

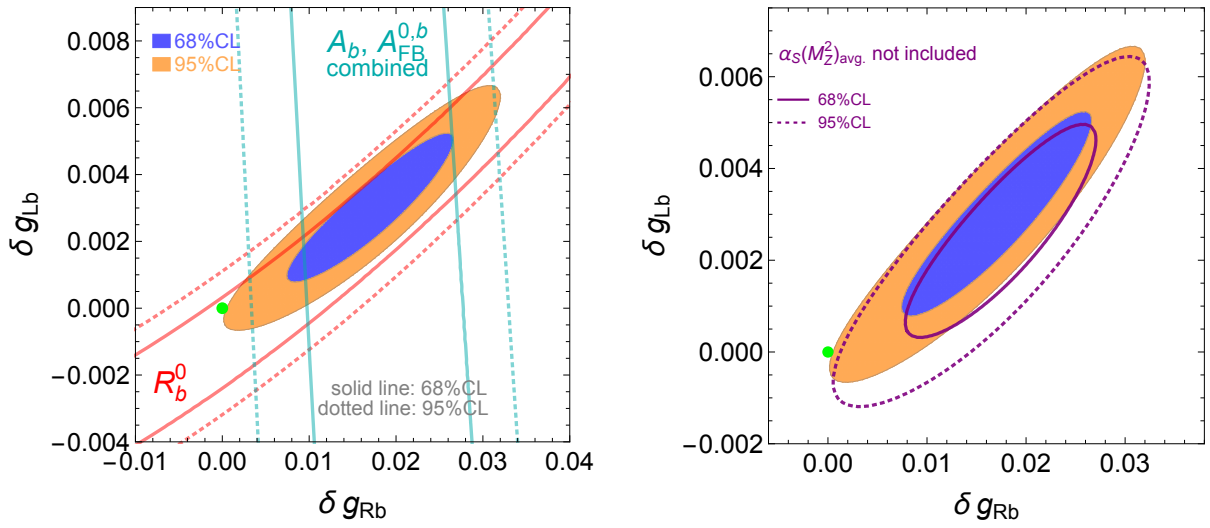

Figure 1: The preferred region in the $(\delta g_{Lb}, \delta g_{Rb})$ plane obtained by the global fit to (SM+$S, T, \delta g_{Lb}, \delta g_{Rb}$) with current data. The blue (orange) region corresponds to the 68% (95%) CL and the green dot is the SM prediction ($\delta g_{Lb} = \delta g_{Rb} = 0$). **Left:** The individual constraints from R_b^0 and from the combination of $\mathcal{A}_b$ and $A_{\rm FB}^{0,b}$ are shown in red and cyan, respectively. For these curves, the parameters other than δg_{Lb} and δg_{Rb} are set to the best-fit values. **Right:** The purple contours show the preferred regions for which $\alpha_S(M_Z^2)_{\rm avg.}$ is not included in the fit. The solid line corresponds to a 68% CL and the dotted line corresponds to a 95% CL.

One can simply extract the value of $\alpha_S(M_Z^2)$ from the EW global fit, which is in good agreement with $\alpha_S(M_Z^2)_{\rm avg.}$ assuming the SM ($+S$ and T). This can be seen by our first two results in Table 2. However, the extraction of $\alpha_S(M_Z^2)$ from EW global fit has some model dependence and, with our model assumption, (SM+$S, T, \delta g_{Lb}, \delta g_{Rb}$), the agreement with $\alpha_S(M_Z^2)_{\rm avg.}$ becomes a bit worse (but still $< 1\sigma$). This result is shown in the last row of Table 2. This suggests that including $\alpha_S(M_Z^2)_{\rm avg.}$ in the fit can have some impact on the $Zb\bar{b}$ coupling constraints. Indeed, as shown in the right plot of Fig. 1, the inclusion of $\alpha_S(M_Z^2)_{\rm avg.}$ has some small but non-negligible effect on δg_{Lb} and on its correlation with δg_{Rb}. This is because $\alpha_S(M_Z^2)_{\rm avg.}$ has a stronger effect on R_b^0 than on $A_{\rm FB}^{0,b}$ and prefers smaller δR_b^0s, leading to an increase in δg_{Lb} and a smaller decrease in δg_{Rb} (see Eq. (2.6)). In the future, while both the precision of the Z-pole data and $\alpha_S(M_Z^2)_{\rm avg.}$ will be improved, $\alpha_S(M_Z^2)_{\rm avg.}$ will at least provide an important consistency check and it will be interesting to include it in the global fit for the $Zb\bar{b}$ coupling constraints.

To summarize this Section, in Table 3 we list both the individual values of and the correlations among $S, T, \delta g_{Lb}, \delta g_{Rb}$ obtained from the global fit of the current precision

model	$\alpha_S(M_Z^2)$ from EW global fit
SM	0.1185 ± 0.0026
SM+(S,T)	0.1180 ± 0.0027
SM+$(S,T,\delta g_{Lb},\delta g_{Rb})$	0.1153 ± 0.0035

Table 2: Prediction for $\alpha_S(M_Z^2)$ from EW global fit with different model assumptions and without the world average $\alpha_S(M_Z^2)_{\text{avg.}} = 0.1185 \pm 0.0005$ as a constraint.

	S	T	δg_{Lb}	δg_{Rb}
S	-0.047 ± 0.097			
T	0.91	0.015 ± 0.077		
δg_{Lb}	-0.34	-0.23	0.0030 ± 0.0015	
δg_{Rb}	-0.40	-0.30	0.91	0.0176 ± 0.0063

Table 3: Best fit values ($\pm 1\sigma$) of and correlations among $S, T, \delta g_{Lb}, \delta g_{Rb}$ from current precision electroweak data, with model assumption being (SM+$S, T, \delta g_{Lb}, \delta g_{Rb}$). A Gaussian distribution is assumed.

electroweak data, with model assumption being (SM+$S, T, \delta g_{Lb}, \delta g_{Rb}$). A given NP model may contribute to both S, T and δg_{Lb}, δg_{Rb}, and to constrain the model one should in principle include all four parameters. However, as shown in Table 3, the correlation between the two groups, (S,T) and $(\delta g_{Lb}, \delta g_{Rb})$, are not very strong, and we expect a similar behavior at future colliders, given that the relative improvements are not extremely different for different observables. For simplicity, in the next Section we shall focus on the constraint on δg_{Lb} and δg_{Rb} and marginalize over S and T. We refer the reader to other literature, e.g. Ref. [5], for prospective constraints on S and T at future e^+e^- colliders.

3 $Zb\bar{b}$ coupling constraints from future e^+e^- colliders

Future e^+e^- colliders will be able to significantly improve the precision of the measurements at the Z-pole thanks to a much larger statistics. The reaches have been estimated in the Technical Design Report (TDR) for ILC [1], the TLEP whitepaper for FCC-ee [2] and the preliminary Conceptual Design Report (preCDR) for CEPC [3]. However, these estimations usually either contain only a subset of EW observables, or have combined several observables into one (*e.g.* the effective leptonic mixing angle $\sin\theta^l_{\text{eff}}$), and are therefore not straight forward to apply in our study. In addition, some of the estimations are rather preliminary, having strong dependence on the assumptions for systematic uncertainties and whether or not beam polarization will be implemented. In Section 3.1, we

outline the key observables that are needed for improving the $Zb\bar{b}$ coupling constraints and try to estimate their precision reach at the three future colliders. Using these estimations, we proceed to study the constraints on the $Zb\bar{b}$ couplings by the method of global fit, and the results are shown in Section 3.2 and 3.3.

In our study we consider the following benchmark scenarios for the three colliders:

- **CEPC** with a relative conservative estimation for the systematic uncertainties and with a statistics of only 2×10^9 Z events. While beam polarization could be a potential option for the run at the Z-pole, here we assume that it is not implemented.
- **CEPC+**, which is CEPC with a more aggressive estimation for the systematic uncertainties, and assuming 10^{10} Z events.
- **ILC**, with a lower statistics (10^9 Z events), but with beam polarization.
- **FCC-ee** with 10^{12} Z events and beam polarization.

3.1 Precision of the EWPOs at future e^+e^- colliders

The observables directly related to the $Zb\bar{b}$ couplings are R_b^0, $A_{\rm FB}^{0,b}$ (measured without beam polarization) and $\mathcal{A}_b$ (measured with beam polarization). However, the three observables also have explicit dependence on the effective weak mixing angles, $\sin^2\theta^l_{\rm eff}$ (for leptons) and $\sin^2\theta^b_{\rm eff}$ (for bottom)[10]. In particular, $A_{\rm FB}^{0,b}$ is quite sensitive to $\sin^2\theta^l_{\rm eff}$ as it is proportional to $\mathcal{A}_e$. In fact, at present, the LEP measurement of $A_{\rm FB}^{0,b}$ provides one of the best determination of $\sin^2\theta^l_{\rm eff}$ assuming SM (the other one being A_{LR} from SLD). Therefore, to extract the $Zb\bar{b}$ couplings from $A_{\rm FB}^{0,b}$, it is important to obtain an independent determination of $\sin^2\theta^l_{\rm eff}$, while the most precise such determination is provided by the leptonic asymmetry observables. On the other hand, R_b^0 and $\mathcal{A}_b$ are numerically not very sensitive to $\sin^2\theta^b_{\rm eff}$.

Without beam polarization, the forward-backward leptonic asymmetry $A_{\rm FB}^{0,l}$ ($= \frac{3}{4}\mathcal{A}_l^2$) can be measured. In addition, a measurement of $\mathcal{A}_l$ ($\mathcal{A}_e$ and $\mathcal{A}_\tau$) can be obtained using the average final-state longitudinal τ polarization and its forward-backward asymmetry [12], which we denote as $\mathcal{A}_l(\mathcal{P}_\tau)$. With beam polarization, the left-right asymmetry A_{LR} ($= \mathcal{A}_e$) can be directly measured, but it is rather irrelevant in terms of the $Zb\bar{b}$ coupling constraints

[10]This can be seen from the tree-level expressions in Eq. (2.4) and Eq. (2.5). The effective weak mixing angle for leptons ($\sin^2\theta^l_{\rm eff}$) and bottom ($\sin^2\theta^b_{\rm eff}$) are not exactly the same due to different loop contributions.

as $\mathcal{A}_b$ can be directly measured as well, and we have checked that the impact of the improvement of A_{LR} on the $Zb\bar{b}$ coupling is rather negligible. However, A_{LR} can still be helpful for constraining the $Zb\bar{b}$ couplings in a global fit, for example, in the case that two (or more) colliders are built and only one of them have beam polarization, similar to the situation of LEP and SLC.

It is worth noting that, apart from R_b^0, a number of additional observables are also sensitive to the coupling combination $g_{Lb}^2 + g_{Rb}^2$ through the dependence on the total hadronic decay width, among which R_l^0, which is the ratio of the total hadronic Z decay width and the Z decay width to one lepton species, is relatively well measured and provides the best sensitivity. We find that a significant improvement of the precision of R_l^0 can have a significant impact on the $Zb\bar{b}$ coupling constraints. In particular, with the estimated precision reach at FCC-ee shown later, the measurement of R_l^0 turns out to be more constraining than the one of R_b^0 to the $Zb\bar{b}$ couplings. However, the constraint from R_l^0 depends strongly on the assumption that the coupling of Z to other fermions are SM-like, and one should be cautious when applying the $Zb\bar{b}$ coupling constraints to a model for which this assumption is not true. In the end of Section 3.2 we will also show the results for FCC-ee with a more conservative estimation for the precision of R_l^0.

To obtain the estimation of the precision reach of the several observables, the following procedure is performed. For each observable, we use the estimation in the corresponding literature, if it is provided. In particular, if a range of values is provided, we choose the more conservative one. If the estimation is not provided in the literature, we estimate the precision with the following strategies: we assume that the systematic uncertainties at CEPC is a factor of 1/3 the ones at LEP and the systematic uncertainties for the scenario "CEPC+" is reduced by an additional factor of 1/2 from CEPC[11]. For CEPC and CEPC+, we assume the statistical uncertainty simply scales with $1/\sqrt{N}$, where N is the total number of Z events expected to be collected. Additionally, for ILC, Ref. [1] does not provide an estimation for the uncertainty of R_l^0 (ΔR_l^0), for which we adopt the estimation in Ref. [18] by Gfitter, $\Delta R_l^0 = 0.004$. Finally, for the FCC-ee, Ref. [2] does not provide an estimation for the uncertainty of $\mathcal{A}_b$ ($\Delta\mathcal{A}_b$). We naïvely scale it from the estimation for the ILC, assuming $\frac{\Delta\mathcal{A}_b}{\Delta A_{LR}}|_{\text{ILC}} \approx \frac{\Delta\mathcal{A}_b}{\Delta A_{LR}}|_{\text{FCC-ee}}$, which gives $\Delta\mathcal{A}_b \approx 0.00021$ at FCC-ee.

[11] An exception of this is the CEPC systematic uncertainty for Rl0(0.006), which we deduced from the total uncertainty (0.007) in the preCDR [3] and then scale to obtain the systematic uncertainty at CEPC+ (0.003).

	Precision				
Observable	Current	CEPC	CEPC+	ILC	FCC-ee
R_b^0 [0.21629]	0.00066 (0.00050)	0.00017 (0.00016)	**0.00008 (0.00008)**	0.00014	0.00006 (0.00006)
R_l^0 [20.767]	0.025 (0.007)	0.007 **(0.006)**	**0.003 (0.003)**	0.004	0.001 (0.001)
$A_{\rm FB}^{0,b}$ [0.0992]	0.0016 (0.0007)	0.00015 (0.00014)	**0.00007 (0.00007)**		
$A_{\rm FB}^{0,l}$ [0.0171]	0.0010 (0.0003)	**0.00014 (0.00010)**	**0.00007 (0.00005)**		
$\mathcal{A}_l(\mathcal{P}_\tau)$ [0.1465]	0.0033 (0.0015)	**0.0006 (0.0005)**	**0.0003 (0.0003)**		
$\mathcal{A}_b$ [0.923]	0.020			0.001	**0.00021 (0.00015)**
A_{LR} [0.1514]	0.0022 (0.0011)			0.0001 (0.0001)	0.000021 (0.000015)
# of Zs	$\sim 2\times 10^7$	$\sim 2\times 10^9$	$\sim 10^{10}$	$\sim 10^9$	$\sim 10^{12}$

Table 4: The estimated precision reach for the observables (which current experimental measurement is shown in the first column) most relevant to constrain the $Zb\bar{b}$ coupling at future colliders. The second column shows the uncertainty of the present measurements from LEP and SLC, while the other columns show the estimations of the precision reach for different future colliders and scenarios. The numbers highlighted in **blue** are our own estimation. In each entry, the number at the top shows the total uncertainty while the number at the bottom (in parenthesis) shows the corresponding systematic uncertainty. A blank entry denotes an observable that is either not measured or not important for our global fit. The last row shows the expected number of Z events that will be collected.

The estimations for the observables mentioned above are summarized in Table 4. A similar method is used to estimate the precision reach for the additional EW observables not listed in Table 4, even if we have checked that they have a much smaller impact on the $Zb\bar{b}$ coupling constraints. In Table 4, the numbers highlighted in **blue** are our own new estimations for those observables not reported in the literature. In each entry, the number at the top shows the total uncertainty while the number at the bottom (in parenthesis) shows the corresponding estimated systematic uncertainty[12]. For comparison, in the second column of the table, we show the current uncertainties, taken from Ref. [12]. A few comments on the table are in order: the systematic uncertainties mostly dominate except for $\mathcal{A}_b$ and A_{LR} at FCC-ee, and for $A_{\rm FB}^{0,l}$ at CEPC. Without beam polarization, CEPC

[12]For some of the observables, only the total experimental uncertainties are quoted in the literature and the entries for the systematic uncertainties are left blank, accordingly.

can not measure $\mathcal{A}_b$ and A_{LR}. For this reason, the corresponding entries are left blank. ILC and FCC-ee can measure $A_{\rm FB}^{0,b}$, $A_{\rm FB}^{0,l}$ and $\mathcal{A}_l(\mathcal{P}_\tau)$, but the corresponding observable with beam polarization, $\mathcal{A}_b$ and A_{LR}, can be measured significantly more precisely, so, for simplicity, we do not include the former observables.

A potential issue for the interpretation of future measurements is the effects of the theoretical uncertainties, which could become important if they are much larger than the experimental uncertainties. In our study, we assume that the electroweak three-loop corrections will be computed in the future. In that case, the effects from the theoretical uncertainties on the $Zb\bar{b}$ coupling constraints are very small and can be safely neglected even for FCC-ee. This is either because the theoretical uncertainty is numerically small (such as $\delta_{\rm th}R_b^0$ which is estimated to be a few times 10^{-5} [6]) or the observable itself has little effect on the $Zb\bar{b}$ coupling constraints, such as the top quark mass. The theoretical uncertainty of $\sin^2\theta_{\rm eff}^b$ also has little impact, since $\mathcal{A}_b$ is not very sensitive to it. More details on the treatment of the theoretical uncertainties can be found in Appendix A.

3.2 SM-like measurements and constraints on NP

In this Section, we assume the future experimental results agree perfectly with the SM predictions and the estimated precision of future measurements as described in the previous Section. The preferred regions in the $(\delta g_{Lb}, \delta g_{Rb})$ plane obtained by our global fit are shown in Fig. 2. The plot in the right panel is a zoomed-in version of the one in the left panel.

From Fig. 2, it is clear that the constraints on the $Zb\bar{b}$ coupling are significantly improved at the future e^+e^- colliders, even for the relatively conservative CEPC estimation (cyan contours), compared to the results of the current precisions (purple contours). With beam polarization, ILC (red contours in the figure) and FCC-ee (black contours in the figure) have better measurements of $\mathcal{A}_b$, which gives a better constraint on δg_{Rb} and also reduce the correlation between δg_{Lb} and δg_{Rb}.

We report the 1σ uncertainties of δg_{Lb} and δg_{Rb} as well as their correlation (ρ) in Table 5. Due to the strong correlation between δg_{Lb} and δg_{Rb} (in particular at CEPC), one need to be careful when using these results to constrain NP models, since in some models only one of δg_{Lb} and δg_{Rb} can receive a sizable contribution while the other one is close to zero. Therefore, in Table 5 we also show the 1σ uncertainties for $\delta g_{Lb}(\delta g_{Rb})$, while $\delta g_{Rb}(\delta g_{Lb})$ is fixed to zero.

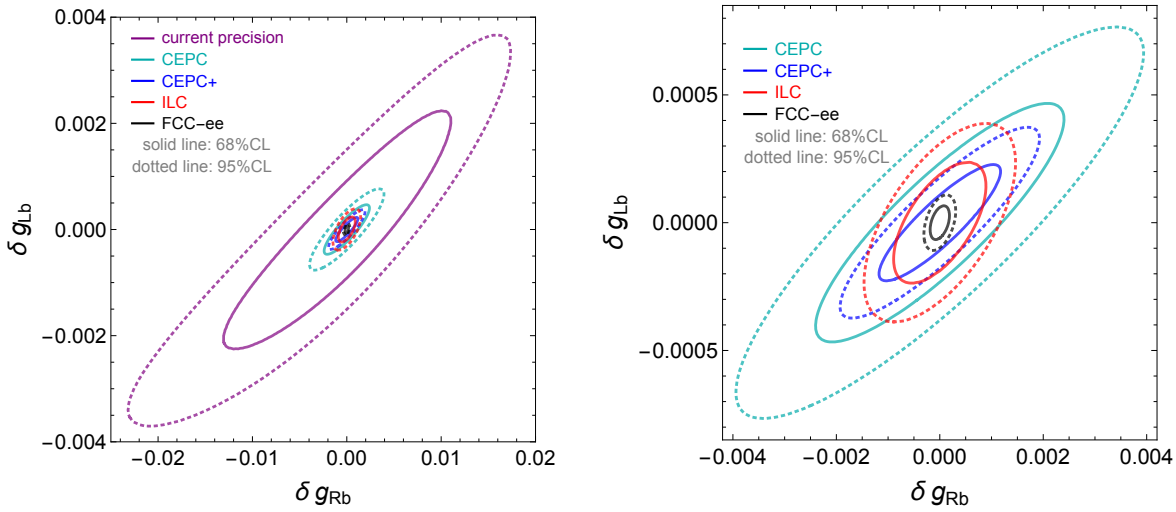

Figure 2: Preferred regions in the $(\delta g_{Lb}, \delta g_{Rb})$ plane, assuming SM central values for all measurements. The model assumption is (SM+$S, T, \delta g_{Lb}, \delta g_{Rb}$), with $S, T, \delta g_{Lb}, \delta g_{Rb}$ all treated as free input parameters. The solid and dotted lines are 68% and 95% CLs, respectively. The purple contours assume current precision for all measurements. The cyan, blue, red and black contours correspond to the estimated precisions for CEPC, CEPC+, ILC and FCC-ee, respectively. The plot in the right panel is a zoomed-in version of the one in the left panel.

For CEPC, the estimation for ΔR_l^0 in the preCDR [3] seems to be very conservative, suggesting little improvement of its systematic uncertainty from LEP to CEPC (see Table 4). A scaling of a factor of 1/3 on the systematic uncertainty would give a value of $\Delta R_l^0 = 0.003$ for the total uncertainty. The results for this scenario are shown in Table 6, which exhibits a slight improvement. In Table 6 we also show the results for FCC-ee with a more conservative estimation of ΔR_l^0, also using $\Delta R_l^0 = 0.003$ (instead of $\Delta R_l^0 = 0.001$).

3.3 Discovering NP through $A_{\rm FB}^{0,b}$ ($\mathcal{A}_b$)

A more interesting possibility is that the long standing $A_{\rm FB}^{0,b}$ discrepancy does come from NP, in which case the precision reach at any of the three future e^+e^- colliders should be able to rule out the SM with very high significance and therefore provide strong indirect evidence for physics beyond SM. To illustrate this point, we consider the following two scenarios. *Scenario I*: we assume that the true values for δg_{Lb} and δg_{Rb} (denoted by δg_{Lb}^0 and δg_{Rb}^0) are given by the best fit values of the current data, $\delta g_{Lb}^0 = 0.0030$ and $\delta g_{Rb}^0 = 0.0176$ (see Table 3). *Scenario II*: we assume that the the true values of δg_{Lb}^0 and δg_{Rb}^0 are closer to zero, while still being consistent with the current measurements within

	δg_{Lb}	δg_{Rb}	ρ	δg_{Lb} $(\delta g_{Rb}=0)$	δg_{Rb} $(\delta g_{Lb}=0)$
current	0.0015	0.0079	0.91	0.00061	0.0032
CEPC	0.00031	0.0016	0.87	0.00015	0.00079
CEPC+	0.00015	0.00078	0.88	0.000072	0.00037
ILC	0.00016	0.00059	0.61	0.00012	0.00047
FCC-ee	0.000044	0.00012	0.42	0.000040	0.00011

Table 5: A comparison of precision reach at different future colliders. The 2nd(3rd) column shows the 1σ uncertainties of $\delta g_{Lb}(\delta g_{Rb})$ while marginalizing over $\delta g_{Rb}(\delta g_{Lb})$. The 4th column shows the correlation (ρ) between δg_{Lb} and δg_{Rb}. The 5th(6th) column shows the 1σ uncertainty of $\delta g_{Lb}(\delta g_{Rb})$ with $\delta g_{Rb}(\delta g_{Lb})$ fixed at zero. We assume future measurements to be in perfect agreement with the SM predictions. A Gaussian distribution is assumed.

$\Delta R_l^0 = 0.003$	δg_{Lb}	δg_{Rb}	ρ	δg_{Lb} $(\delta g_{Rb}=0)$	δg_{Rb} $(\delta g_{Lb}=0)$
CEPC	0.00031	0.0015	0.93	0.00011	0.00057
FCC-ee	0.000051	0.00012	0.32	0.000048	0.00012

Table 6: Same as Table 5, but for CEPC and FCC-ee both with $\Delta R_l^0 = 0.003$, which serves as a reasonably optimistic estimation for CEPC and a conservative one for FCC-ee.

68%CL. As a benchmark point, we choose $\delta g_{Lb}^0 = 0.0009$ and $\delta g_{Rb}^0 = 0.0075$. In principle, one would expect the NP to have non-zero contributions to the S and T parameters, as well. We find that changing the central values of S and T of the hypothetical measurement within the current constraints has very small impact on the $Zb\bar{b}$ couplings. For simplicity we assume that the hypothetical data agrees with SM other than the modification to g_{Lb} and g_{Rb}.

The preferred regions in the $(\delta g_{Lb}, \delta g_{Rb})$ plane are shown in Fig. 3. The two plots correspond to the two scenarios described above, and each shows the 99.9999% CL (corresponding to 5σ for a one-dimensional Gaussian distribution) constraints from different colliders. From the figure, it is clear that the SM prediction at zero (denoted by a green dot) can be ruled out at 99.9999% CL by all the e^+e^- colliders we discuss, even if we assume that the future measurements will point towards smaller values of δg_{Lb} and δg_{Rb} within 68% CL of the current measurements.

4 Implication on NP models

In this Section, we analyze the implications of the future measurements of the $Zb\bar{b}$ couplings on specific NP models. We start with a brief discussion of the constraints on

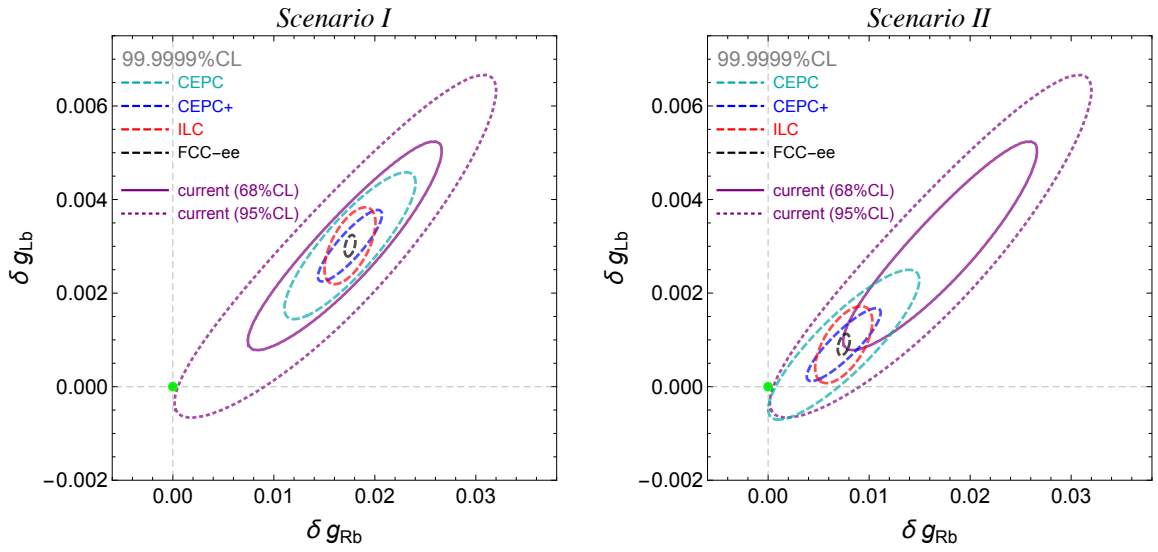

Figure 3: The preferred regions in the $(\delta g_{Lb}, \delta g_{Rb})$ plane, given by the global fit of the future measurements at CEPC (in cyan), CEPC+ (in blue), ILC (in red) and FCC-ee (in black). The solid and dotted purple contours correspond to the 68% and 95% CL constraints from the current measurements. The two panels correspond to *Scenario I* and *Scenario II* presented in the text, and each plot shows the 99.9999% CL constraints from different colliders with dashed contours. The green dot is the SM prediction ($\delta g_{Lb} = \delta g_{Rb} = 0$).

effective Lagrangians. At dimension 6, the only operators that modifies directly the $Zb\bar{b}$ couplings are (see e.g. [17, 21])

$$\mathcal{O}_{Hb} = i(H^\dagger \overleftrightarrow{D}_\mu H)(\bar{b}_R \gamma^\mu b_R)\,, \tag{4.1}$$

$$\mathcal{O}^s_{HQ} = i(H^\dagger \overleftrightarrow{D}_\mu H)(\bar{Q} \gamma^\mu Q)\,, \tag{4.2}$$

$$\mathcal{O}^t_{HQ} = i(H^\dagger \sigma^a \overleftrightarrow{D}_\mu H)(\bar{Q} \gamma^\mu \sigma^a Q)\,. \tag{4.3}$$

After electroweak symmetry breaking, these operators lead to a shift in the $Zb\bar{b}$ couplings:

$$\delta g_{Lb} = -\frac{(a^s_{HQ} + a^t_{HQ})v^2}{2}\,, \qquad \delta g_{Rb} = -\frac{a_{Hb} v^2}{2}\,, \tag{4.4}$$

where a_{Hb}, a^s_{HQ}, a^t_{HQ} are the coefficients of the $\mathcal{O}_{Hb}$, $\mathcal{O}^s_{HQ}$, $\mathcal{O}^t_{HQ}$ operators, respectively and v is the vacuum expectation value of the Higgs ($v = 246$ GeV). In Table 7, we present the constraints on these operators at the several future e^+e^- machines, assuming that $a^s_{HQ} = a^t_{HQ} = a_{Hb} = 1/\Lambda^2$. Scales as large as $(20 - 30)$ TeV can be probed by the future measurement of the $Zb\bar{b}$ couplings.

Next, we pass to the analysis of specific NP frameworks that can generate some of the operators forementioned, including two Higgs doublet models, composite Higgs models

	current	CEPC	CEPC+	ILC	FCC-ee
Λ(TeV)	6.8	13	20	15	27

Table 7: 95%CL bounds on the cutoff scale Λ from different future colliders, using the results from Section 3.2 and assuming that $a^s_{HQ} = a^t_{HQ} = a_{Hb} = 1/\Lambda^2$.

and the Beautiful Mirror Model. It should be noted that for natural SUSY with minimal ingredients, the $Zb_L\bar{b}_L$ coupling receives corrections from loops involving stops and Higgsinos, while they are rather small for the future measurements of the $Zb\bar{b}$ to have an impact, as shown e.g. in Ref. [6].

4.1 Two Higgs doublet models

As shown in e.g. [11], models with an extended Higgs sector can predict sizable NP contributions to the $Zb\bar{b}$ vertex. In particular, focusing on two Higgs doublet models (2HDMs), based on discrete symmetries to avoid flavor changing neutral currents (FCNCs) at the tree level, the most important contribution generically comes at the one loop level, from the charged Higgs exchange. The sign of the charged Higgs NP contribution to δg_{Lb} (δg_{Rb}) is fixed and is always positive (negative). In a Type II 2HDM, the contribution to δg_{Lb} (δg_{Rb}) increases at small (large) values of $\tan\beta$, since the coupling $H^\pm\bar{b}_L t_R$ ($H^\pm\bar{t}_L b_R$) leading to a non-zero δg_{Lb} (δg_{Rb}) is proportional to $m_t/\tan\beta$ ($m_b\tan\beta$). In a Type I 2HDM, instead, both δg_{Lb} and δg_{Rb} increase at large values of $\tan\beta$[13], leading always to a NP contribution $\delta g_{Lb} \gg \delta g_{Rb}$. In Fig. 4, we show the constraints on the $m_{H^\pm} - \tan\beta$ plane, using the present measurement of the $Zb\bar{b}$ coupling (in purple) as well as the expected more precise measurement at CEPC (in cyan), CEPC+ (in blue), ILC (in red) and FCC-ee (in black). For the figure, we have assumed that the future measurements perfectly agree with the SM predictions and we have marginalized over the values of the S and T parameters.

In Type II models, interesting constraints arise at low values of $\tan\beta$ for which $\delta g_{Lb} \gg \delta g_{Rb}$[14]. Type I models, instead, are only allowed in the region with small $\tan\beta$ unless $m_{H^\pm}$ is very large. If we specify the full spectrum of a 2HDM, including the masses of the

[13]Here we use the $\tan\beta$ convention such that the two charged Higgs couplings are proportional to $m_t\tan\beta$ and $m_b\tan\beta$.

[14]In a Type II 2HDM, only very large values of $\tan\beta$ can be excluded by the measurement of δg_{Rb}: $\tan\beta \sim \mathcal{O}(50)$ (30) for $m_{H^\pm} \sim 200$ GeV at CEPC+ (FCC-ee). At large $\tan\beta$, the exact exclusion depends also on the neutral Higgs spectrum, since in this case the neutral and charged Higgses give a parametrically similar contribution to δg_{Lb} and δg_{Rb}.

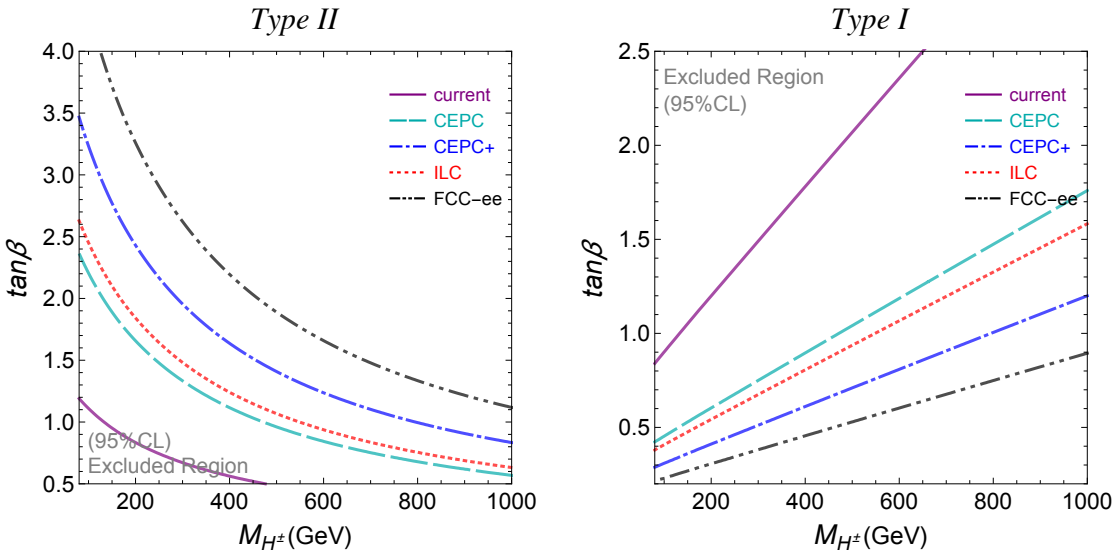

Figure 4: Constraints on the charged Higgs parameter space in a Type II 2HDM (left panel) and in a Type I 2HDM (right panel). In purple is the constraint we obtain using the present uncertainties on the EWPOs; in cyan, blue, red and black are the constraints expected with the future measurements at CEPC, CEPC+, ILC and FCC-ee, respectively. In the Type II 2HDM, the region below the curves is excluded. In the Type I 2HDM, the exclusion is above the curves. We assume that the future measurements perfectly agree with the SM predictions and marginalized over the values of the S and T parameters.

neutral scalar H and pseudoscalar A, as well as the mixing angle $\alpha - \beta$ between the two doublets, S and T are not free parameters. In general, the constraints will be stronger. As an example, in a type II 2HDM, if we fix $m_A = m_H = 200$ GeV, $m_{H^\pm} = 150$ GeV and $\cos(\alpha - \beta) = 0.1$, then the model gives $S \sim 0.02$ and $T \sim 0.04$. For this specific set of parameters, the CEPC bound on $\tan\beta$ is ~ 2, instead of ~ 1.8, as presented in the left panel of Fig. 4 (see the cyan dashed line).

Presently, LHC charged Higgs searches almost totally exclude charged Higgs bosons with a mass below the top mass in Type II 2HDMs [33]. There are no LHC searches at around the top mass, for $160\,\text{GeV} < m_{H^\pm} < 180$ GeV up to date. Above 180 GeV, constraints are rather weak and cover only models with large values of $\tan\beta$ ($\tan\beta \geq 40$), for which the production cross section of the charged Higgs in association with a top quark is in the $\mathcal{O}(1)$ pb range. In this regime, the two most important bounds come from the searches for $H^\pm \to \tau\nu$ [33] and for $H^\pm \to tb$ [34]. At the 14 TeV LHC, also charged Higgs boson with mass above the top mass will be relatively well probed. In particular, searches for $H^\pm \to tb$ will have the potential to probe $\tan\beta \lesssim 3$ and $\tan\beta \gtrsim 15$ for $m_{H^\pm} \sim 500$ GeV at the High Luminosity (HL)-LHC [35]. Comparing to our results of

Fig. 4 (left panel), we see that constraints from future measurements of EWPOs can be complementary to direct searches for Type II 2HDMs, being able to probe low values of $\tan\beta$ even for $m_{H^\pm} \gg m_t$, as well as the challenging region $160\,\text{GeV} < m_{H^\pm} < 180$ GeV, presently not covered by direct searches.

Finally, one can interpret the searches for charged Higgs bosons in terms of Type I 2HDMs. Below the top mass, only a small region with $\tan\beta < 1$ has not been yet probed by the $H^\pm \to \tau\nu$ search. Above the top mass, the exclusion is very week and is not covering any part of the plane shown in Fig. 4 (right panel). At the HL-LHC, this region will be very well probed by a $H^\pm \to tb$ search, with potential exclusions for the entire range of $\tan\beta$ presented in the figure, up to $m_{H^\pm} \sim 500$ GeV.

4.2 Composite Higgs models

Composite Higgs models usually predicts a large correction to the $Zb_L\bar{b}_L$ coupling, since a sizable mixing between the third generation quarks and the strong dynamics is needed to generate the large top mass. The correction to the $Zb_R\bar{b}_R$ coupling is usually much smaller, unless one specifically extend the fermion sector to generate a large correction (*e.g.*, as in Ref. [36]). It was pointed out in Ref. [10] that an $O(4)$ symmetry, which is the $SU(2)_L \otimes SU(2)_R$ symmetry, analogous to the custodial symmetry protecting the weak isospin, with the addition of a left-right parity P_{LR}, could be used to protect the $Zb_L\bar{b}_L$ coupling, such that a natural composite Higgs model can be consistent with EW precision constraints. Nevertheless, in realistic models there still exist corrections to the $Zb_L\bar{b}_L$ coupling because 1) the P_{LR} symmetry can only protect the $Zb_L\bar{b}_L$ coupling at zero momentum and 2) there are also several contributions that explicitly break P_{LR}. These corrections could become relevant if the constraint on the $Zb_L\bar{b}_L$ coupling is significantly improved at future e^+e^- colliders. Ref. [37] estimates the size of different contributions to the $Zb_L\bar{b}_L$ coupling in minimal composite Higgs models with custodial protection. (Also see Ref. [38] for a recent review.) While the magnitudes and signs of different contributions are rather model dependent, the leading correction usually comes from P_{LR} breaking effects of fermion loops and is

$$\frac{\delta g_{Lb}}{g_{Lb}^{\text{SM}}} \simeq \frac{y_t^2}{16\pi^2}\frac{v^2}{f^2}\log\left(\frac{m_\rho^2}{m_4^2}\right), \tag{4.5}$$

where y_t is the top Yukawa coupling, m_ρ is the mass of the ρ meson which cuts off the loop correction, and m_4 is the mass of the 4-plet composite quarks which is essentially the mass of the (lightest) top partner up to some corrections from mixing. Taking Eq. (4.5)

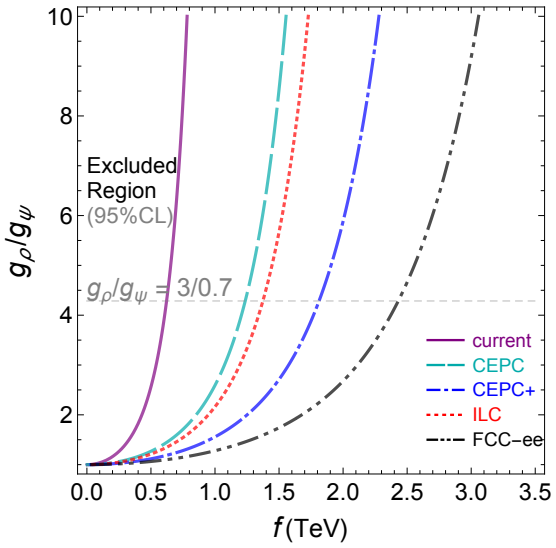

Figure 5: Constraints in the $(g_\rho/g_\psi, f)$ plane assuming the only correction to the $Zb\bar{b}$ couplings are given by Eq. (4.5). Each contour represents the 95% CL constraint and the region in the top-left side of the contour is excluded. The grey horizontal line corresponds to $g_\rho/g_\psi = 3/0.7$. In purple is the constraint we obtain using the present uncertainties on the EWPOs; in cyan, blue, red and black are the constraints expected with the future measurements at CEPC, CEPC+, ILC and FCC-ee, respectively.

as an equality, the results in Table 5 (assuming $\delta g_{Rb} = 0$) can be interpreted in terms of constraints in the $(g_\rho/g_\psi, f)$ plane where $g_\rho \equiv m_\rho/f$ and $g_\psi \equiv m_4/f$. This is shown in Fig. 5, where each contour represents the 95% CL constraint and the region in the top-left side of the contour is excluded. The grey horizontal line has $g_\rho/g_\psi = 3/0.7$ which corresponds to the benchmark point $m_\rho = 3$ TeV and $m_4 = 700$ GeV of Ref. [37].

Since g_ρ/g_ψ is typically bounded to be a few times one, future e^+e^- colliders can constrain f to be at least a few TeVs thanks to the measurement of the $Zb\bar{b}$ couplings. This is comparable to the constraints from the direct searches of top partners at the next run of the LHC, given that the mass of the top partner can not be much larger than f in order to obtain the correct Higgs mass [39]. The constraints from the $Zb\bar{b}$ couplings is significantly stronger than the ones from oblique parameters but weaker than the ones from Higgs precision measurement, and in particular from the HZZ vertex, quoted in Ref. [5]. The latter can, in fact, constrain f at the level of ~ 2.8 TeV (CEPC) and ~ 3.9 TeV (FCC-ee) at 95%CL. Other studies of future constraints on composite Higgs models can be found in Ref. [40, 41]. To conclude, while the constraints from $Zb\bar{b}$ couplings has a stronger model dependence, it is complementary to the constraints from

oblique corrections, Higgs precision measurements and direct searches and can be very helpful for the discrimination of different composite Higgs models.

4.3 The Beautiful Mirror Model

In the Beautiful Mirror Model proposed in Ref. [32], the modifications to the $Zb\bar{b}$ couplings are caused by the mixing of the bottom quark and new heavy vector-like quark(s)[15]. In the simplest case with only one bottom-partner B, the shifts in the couplings are given by $\delta g_{Lb} = (t_3 + 1/2)s_L^2$ and $\delta g_{Rb} = t_3 s_R^2$, where t_3 is the charge of the new bottom quark, B, under $SU(2)_L$ and $s_{L(R)}$ is the sine of the left(right)-handed mixing angle between the SM b quark and B. To obtain a shift in g_{Rb}, the new quark B can not be a $SU(2)_L$ singlet. If B has $t_3 = -\frac{1}{2}$, δg_{Rb} would be negative and one would need a large shift in the coupling to flip its sign, $g_{Rb} \approx -g_{Rb}^{\rm SM}$, in order to resolve the $A_{\rm FB}^{0,b}$ discrepancy. Such a large shift requires a very light B quark and a large custodial symmetry breaking and has been almost completely probed by LHC direct searches for vector-like quarks [16, 43, 44]. A more appealing choice is $t_3 = \frac{1}{2}$, that can lead to a good fit of the EWPOs, without a too light B quark, thanks to a positive contribution to g_{Rb}. This scenario was denoted as the "Top-less Mirror" in the original paper [32], since there is no top-partner in the new doublet quark. The new doublet quark alone can not simultaneously generate a sizable enough δg_{Lb}, but this can be easily achieved by introducing an additional singlet. Therefore, we discuss an extension of the SM with the following vector-like quarks,

$$\Psi_{L,R} = \begin{pmatrix} B \\ X \end{pmatrix} \sim (3, 2, -5/6)\,, \tag{4.6}$$

$$\hat{B}_{L,R} \sim (3, 1, -1/3)\,, \tag{4.7}$$

where the numbers in the bracket denotes representations under $SU(3)_c$, $SU(2)_L$, and the $U(1)_Y$ hypercharge. The relevant terms in the Lagrangian are given by

$$-\mathcal{L} \supset M_1 \bar{\Psi}_L \Psi_R + M_2 \bar{\hat{B}}_L \hat{B}_R + y_1 \bar{Q}_L H b_R + y_L \bar{Q}_L H \hat{B}_R + y_R \bar{\Psi}_L \tilde{H} b_R + \text{h.c.}\,, \tag{4.8}$$

which leads to the following 3×3 mass matrix $\mathcal{M}_B$ for the bottom-like quarks while the mass of the charge $-4/3$ quark X is simply given by M_1,

$$\mathcal{M}_B = \begin{pmatrix} Y_1 & 0 & Y_L \\ Y_R & M_1 & 0 \\ 0 & 0 & M_2 \end{pmatrix}, \qquad \mathcal{M}_X = M_1\,, \tag{4.9}$$

[15] See also [42] for a more recent analysis of the fit of the $Zb\bar{b}$ couplings in models with vector-like quarks.

where $Y_i = \frac{y_i v}{\sqrt{2}}$. The shifts in the $Zb\bar{b}$ couplings are thus given by

$$\delta g_{Lb} = \frac{Y_L^2}{2M_2^2}\,, \qquad \delta g_{Rb} = \frac{Y_R^2}{2M_1^2}\,. \tag{4.10}$$

The new quarks contributes also to the T parameter through fermion loops. Ignoring the small bottom mass and the higher order terms, the T parameter is given by

$$T \approx \frac{3}{16\pi^2 \alpha v^2}\left[\frac{16}{3}\delta g_{Rb}^2 M_1^2 + 4\delta g_{Lb}^2 M_2^2 - 4\delta g_{Lb}\frac{M_2^2\, m_{\rm top}^2}{M_2^2 - m_{\rm top}^2}\log\left(\frac{M_2^2}{m_{\rm top}^2}\right)\right]. \tag{4.11}$$

If δg_{Lb} and δg_{Rb} are fixed to non-zero values, as preferred by the current EW measurements, the T parameter will increase if one increases the mass scales of the new quarks, as shown in the left plot of Fig. 6. This is because larger Yukawa couplings are needed if one wants to fix δg_{Lb} and δg_{Rb} while increasing M_1 and M_2, as shown in Eq. (4.10). Since the desired value of δg_{Rb} is much larger than the one of δg_{Lb}, the T parameter is more sensitive to M_1. The contribution to the S parameter is very small in this model, and we assume it to be zero for simplicity. The right plot of Fig. 6 (solid blue line) shows the value of $\Delta\chi^2$ (measured from the minimum χ^2 that can be reached in this model) as a function of M_1, obtained from the global fit of the current EW precision data, while other model parameters are chosen to minimize $\Delta\chi^2$ for a given value of M_1. At small M_1 ($\lesssim 1.4$ TeV), one could tune the value of M_2 to obtain the best-fit value of the T parameter (≈ 0.05 if fixing $S = 0$). For larger values of M_1, the agreement with data is significantly worse due to the tension between the T parameter and δg_{Rb}. For comparison, we also show the $\Delta\chi^2$ curve for CEPC (dashed red curve), assuming that the central values of S, T, δg_{Lb}, δg_{Rb} are the same as the current ones: CEPC will tightly constrains M_1 to be below ~ 1.6 TeV.

An additional upper bound on M_1 can be obtained by requiring the theory to be perturbative. In particular, Eq. (4.10) implies $y_R \approx 2\sqrt{\delta g_{Rb}}\frac{M_1}{v}$. Assuming the true values of δg_{Lb} and δg_{Rb} are within 68% CL of the current measurements, we have $\delta g_{Rb} \gtrsim 0.0075$ and hence

$$y_R \gtrsim \frac{M_1}{1.4\ \text{TeV}}\,. \tag{4.12}$$

Therefore, M_1 can not be much larger than a few TeV without the Yukawa coupling, violating perturbativity bounds.

The LHC is directly searching for the mirror quarks. As pointed out in Ref. [44], the charge $-4/3$ exotic quark X decays to b and W with the same sign of electric charges, which is extraordinary in theory but hard to capture in experiments, since it is very hard

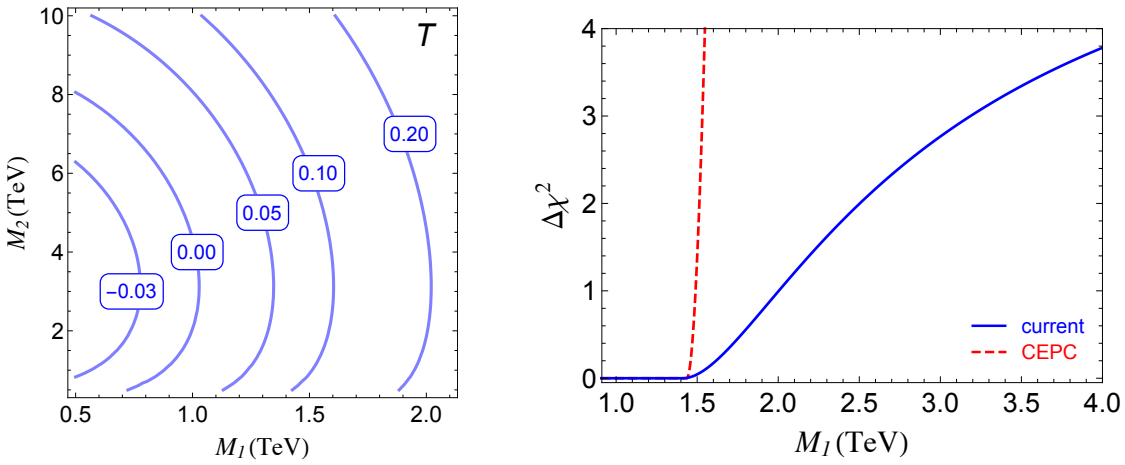

Figure 6: **Left**: The value of T parameter in the (M_1, M_2) plane, while δg_{Lb} and δg_{Rb} are fixed to the current best fit values, $\delta g_{Lb} = 0.0030$ and $\delta g_{Rb} = 0.0176$. **Right**: $\Delta\chi^2$ as a function of M_1, obtained from the global fit of the EW precision data to the model while marginalizing over other model parameters. The $\Delta\chi^2$ is measured from the minimum χ^2 that can be reached in this model. The solid blue line is obtained from the current data; the dashed red line is from hypothetical CEPC data, while we naïvely assume that the central values of S, T, δg_{Lb}, δg_{Rb} are the same as the current ones. The horizontal axis starts at 912 GeV, the current 95% CL bound from the direct searches of vector-like quarks at the 8 TeV LHC.

(if not impossible) to measure the charge of b-jets. As such, the strongest bounds on X come from searches of top partners decaying to bW. The recent CMS analysis [45] sets a lower limit of 912 GeV at the 95% CL for a pair produced top vector-like quark with 100%BR to bW, using 8 TeV data. Currently, this is the most stringent constraint on M_1. There also exist bounds from bottom partner searches (*e.g.* Ref. [46]) which are slightly weaker.

The current constraint from the LHC is consistent with the one from EW precision data shown in the right plot of Fig. 6. The situation may get much more interesting in the future: the bounds on the mirror quark masses are expected to reach (2-2.5) TeV at the 14 TeV LHC [44, 47] using the single production channel. The HL-LHC with $3000\,\text{fb}^{-1}$ data could probably push the bound further to above 3 TeV, if the data is consistent with SM [48]. Such a bound would be in tension with the current EW precision data. If no mirror quark is found during the LHC run, it could be an indication that either 1) the LEP $A_{\text{FB}}^{0,b}$ discrepancy is not due to NP or it comes from some NP other than the

Beautiful Mirror Model[16] or 2) the underlying NP is some extension or modification of the "minimal" Beautiful Mirror Model which evades the constraints from direct searches, still producing a good fit to EW precision data.

Finally, we comment on the fact that the Beautiful Mirror Model predicts a significant modification to the $hb\bar{b}$ and hgg couplings [16],

$$\frac{y_{hb\bar{b}}}{(y_{hb\bar{b}})_{\rm SM}} \simeq 1 - 2(\delta g_{Lb} + \delta g_{Rb})\,, \qquad \frac{g_{hgg}}{(g_{hgg})_{\rm SM}} \simeq 1 + 2(\delta g_{Lb} + \delta g_{Rb})\,. \tag{4.13}$$

The current best-fit values of δg_{Lb} and δg_{Rb} predict a $\sim 4\%$ deviation on the $hb\bar{b}$ and hgg couplings which will be detectable at a future Higgs Factory [1–3].

5 Conclusion

Precision measurements of SM couplings are the central goal of future lepton colliders. Such measurements are complementary to direct searches at high energy proton colliders. In this paper, we have extracted the constraints on possible modifications of the $Zb\bar{b}$ couplings from the SM predictions by performing global fits of both the current precision data and the prospective data from future e^+e^- colliders. We pointed out that the world average value of the strong coupling constant contains non-trivial information and should be included in the global fit of models with non-zero NP contributions to the $Zb\bar{b}$ vertex, which has not been pointed out elsewhere. For the future colliders, we summarized the set of observables most important for improving the $Zb\bar{b}$ coupling constraints and compared the precision reaches at CEPC, ILC and FCC-ee. We studied both the case that the results are SM-like and the one that the $Zb\bar{b}$ couplings deviate significantly from the SM prediction as suggested by the LEP $A_{\rm FB}^{0,b}$ discrepancy. For the latter case, we showed that even if we assume that the future measurements will point towards smaller values of δg_{Lb} and δg_{Rb} within 68% CL of the current measurements, any one of the proposed e^+e^- colliders will be able to rule out the SM with more than 99.9999% CL, equivalent to 5 standard deviations for a one-dimensional Gaussian distribution.

Finally, we studied the implication on NP models from the improvements of the $Zb\bar{b}$ coupling constraints. We first considered generic 2HDMs, in which the limits from precision $Zb\bar{b}$ measurements are complementary to those from the LHC searches of charged

[16] Another possible solution would be a Z' near Z-pole, as proposed in Ref. [49, 50]. Future e^+e^- colliders could perform a much better scan around the Z-pole compared with LEP and provide significantly better discriminating power between the SM and this scenario.

Higgs bosons. In particular, future measurements of the $Zb\bar{b}$ vertex will be able to test Type II 2HDMs at low values of $\tan\beta$ ($\tan\beta \lesssim 1-4$), even in the mass range $160\,\text{GeV} < m_{H^\pm} < 180$ GeV, presently not covered by direct LHC searches. We then considered composite Higgs models, where deviations in the $Zb\bar{b}$ couplings are generically expected. Measurement at future lepton colliders can probe composite resonances with masses of multiple TeVs, possibly beyond the reach of the LHC. Finally, in the literature there have been new physics models motivated by the long standing LEP anomaly in $A_{\text{FB}}^{0,b}$. As an example, we considered the so called Beautiful Mirror Model in which new fermions mix with the SM bottom quark. We find that, for the minimal scenario, future precision measurements of $Zb\bar{b}$ could put a strong upper bound on the new fermion masses at around 1.6 TeV, if the measured central values of S, T, δg_{Lb} and δg_{Rb} are the same as the current ones. Future LHC searches of vector-like quarks will be able to fully probe this mass range.

We have also shown that the particular models considered in this paper generically predict deviations in the Higgs couplings, which can also be measured very precisely at the Higgs factory stage of the lepton colliders. The interplay between Higgs and Z precision measurements will be very valuable at future e^+e^- machines, in extracting maximal information about new physics.

Acknowledgments

We would like to thank Jens Erler for discussion. The research of SG at Perimeter Institute is supported by the Government of Canada through Industry Canada and by the Province of Ontario through the Ministry of Economic Development & Innovation. SG acknowledge support by the Munich Institute for Astro- and Particle Physics (MIAPP) of the DFG cluster of excellence *Origin and Structure of the Universe*. JG is supported in part by the Chinese Academy of Science (CAS) International Traveling Award under Grant H95120N1U7 and the CAS Center for Excellence in Particle Physics (CCEPP). LTW acknowledges the hospitality of the Center for Future High Energy Physics (CFHEP) where part of this work was done.

A Theoretical uncertainties

We follow Ref. [5] for the treatment of theoretical uncertainties, which we discuss in this Appendix. Given a set of model parameters $\boldsymbol{\theta}$, the true value of a particular observable

x is predicted to be some certain value, $x_{\rm th}$, up to some uncertainty, δ. This uncertainty could come from the omission of higher order terms in a fixed order calculation, or the subtlety in the definition of certain quantities (*e.g.* the top mass). As such, it is strictly speaking not a statistical quantity and there is no good reason to assume it follows a Gaussian distribution. We assume x takes a probability density function $h(x;\boldsymbol{\theta})$ that is flat within $x_{\rm th} \pm \delta$ and zero elsewhere,

$$h(x;\boldsymbol{\theta}) = \begin{cases} \frac{1}{2\delta} & \text{if } |x - x_{\rm th}| \leq \delta \\ 0 & \text{if } |x - x_{\rm th}| > \delta \end{cases} . \tag{A.1}$$

On the other hand, we assume the measured value, $x_{\rm mea}$, takes a Gaussian distribution $g(x_{\rm mea}|x)$ centered around the true value x with standard deviation σ.

The distribution of the measure value $x_{\rm mea}$ given a set of model parameters $\boldsymbol{\theta}$ is thus obtained by convolution:

$$\begin{aligned} f(x_{\rm mea};\boldsymbol{\theta}) =& \int dx\ g(x_{\rm mea}|x) h(x;\boldsymbol{\theta}) \\ =& \frac{1}{4\delta}\left(\text{erf}\Big(\frac{x_{\rm mea} - x_{\rm th} + \delta}{\sqrt{2}\sigma}\Big) - \text{erf}\Big(\frac{x_{\rm mea} - x_{\rm th} - \delta}{\sqrt{2}\sigma}\Big)\right) , \end{aligned} \tag{A.2}$$

which reduces to the Gaussian distribution in the limit $\delta \to 0$. Eq. (A.2) can be implemented in a global fit with N observables with a modified χ^2 function (assuming no correlation)

$$\chi^2_{\rm mod} = \sum_{j=1}^{N} \left[-2\log\left(\frac{1}{4\delta_j}\left(\text{erf}\left(\frac{M_j - O_j + \delta_j}{\sqrt{2}\sigma_j}\right) - \text{erf}\left(\frac{M_j - O_j - \delta_j}{\sqrt{2}\sigma_j}\right)\right)\right) - 2\log\left(\sqrt{2\pi}\sigma_j\right)\right] , \tag{A.3}$$

where for each observable j, M_j is the measured value, O_j is the predicted value, σ_j is the experimental uncertainty and δ_j is the theoretical uncertainty. R_b^0 and $A_{\rm FB}^{0,b}(\mathcal{A}_b)$ are directly related to the $Zb\bar{b}$ couplings, and their theoretical uncertainties are most important to our study. The theoretical uncertainty of R_b^0 ($\delta_{\rm th}R_b^0$) is estimated to be 1.5×10^{-4} from two-loop diagrams without closed fermion loops and higher-order contributions [15] and could be reduced to a few times 10^{-5} assuming the 2-loop and 3-loop computations will be completed in the future [6]. Naively, one would expect it to have an impact, especially for FCC-ee which will be able to measure R_b^0 to a precision of about 6×10^{-5}. However, even with a conservative estimation, $\delta_{\rm th}R_b^0 = 5 \times 10^{-5}$, and for FCC-ee, we find the change of the total uncertainty from the inclusion of the theoretical uncertainty rather small, as the 68% CL bound changes from 6×10^{-5} to 6.65×10^{-5}. The corresponding probability density functions are shown in Fig. 7, for which we have set the central value

to zero and scaled up the uncertainties by 10^5 for convenience. Given that the estimations of the future experimental uncertainties are still very preliminary, we ignore this small effect due to the theoretical uncertainty of R_b^0 in our study.

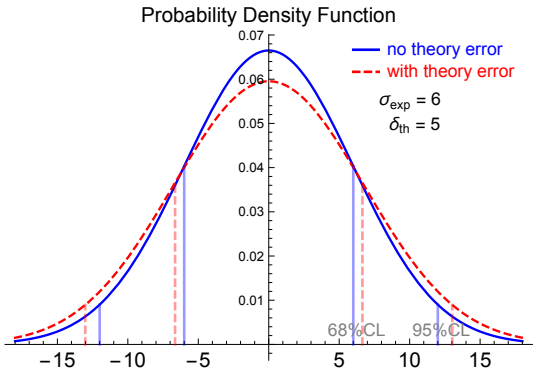

Figure 7: Probability Density Functions (p.d.f.) for theoretical uncertainty $\delta_{\rm th} = 5$, experimental uncertainty $\sigma_{\rm exp} = 6$ and the combined total uncertainty, assuming a zero central value. The blue solid line shows the p.d.f. with the experimental uncertainty only, which follows a Gaussian distribution. The red dashed line shows the p.d.f. with experimental and theoretical uncertainties combined with Eq. (A.2). The light vertical lines shows the corresponding 68% and 95% CL bounds. Without the theoretical uncertainty, the 68% and 95% CL bounds are ± 6 and ± 12; with the theoretical uncertainty, the 68% and 95% CL bounds are ± 6.65 and ± 13.0.

With (longitudinal) beam polarization, $\mathcal{A}_b$ can be directly measured. Without beam polarization, $A_{\rm FB}^{0,b}$ can be measured, which is related to $\mathcal{A}_b$ by $A_{\rm FB}^{0,b} = \frac{3}{4}\mathcal{A}_e\mathcal{A}_b$. The value of $\mathcal{A}_e$ can be extracted experimentally by the measurement of $A_{\rm FB}^{0,l}$. Therefore, the theoretical uncertainty of $A_{\rm FB}^{0,b}$ also only comes from $\mathcal{A}_b$, which can be parameterized by the theoretical uncertainty of $\sin^2\theta_{\rm eff}^b$ (The overall form factors of g_{Lb} and g_{Rb} cancel in the ratio.) $\mathcal{A}_b$ is numerically not very sensitive to $\sin^2\theta_{\rm eff}^b$. At the leading order in the SM, one has

$$\delta_{\rm th}\mathcal{A}_b \approx -0.64\,\delta_{\rm th}\sin^2\theta_{\rm eff}^b\,, \qquad \delta_{\rm th}A_{\rm FB}^{0,b} \approx -0.070\,\delta_{\rm th}\sin^2\theta_{\rm eff}^b\,, \tag{A.4}$$

where $\delta_{\rm th}$ denotes the theoretical uncertainty of the corresponding quantity. Even with the current theoretical uncertainty of $\sin^2\theta_{\rm eff}^b$, which is about 5×10^{-5} [51], $\delta_{\rm th}\mathcal{A}_b$ and $\delta_{\rm th}A_{\rm FB}^{0,b}$ are much smaller than the future experimental precisions and can be safely ignored.

The effects of the theoretical uncertainties of other quantities, such as the top mass and W mass, are important in general (*e.g.* for the S and T parameters, as pointed out in Ref. [5]) but do not directly affect the $Zb\bar{b}$ couplings. We implemented these theoretical uncertainties and found that the changes of the $Zb\bar{b}$ coupling constraints are negligible.

References

[1] H. Baer, T. Barklow, K. Fujii, Y. Gao, A. Hoang, et al., *The International Linear Collider Technical Design Report - Volume 2: Physics*, arXiv:1306.6352.

[2] **TLEP Design Study Working Group** Collaboration, M. Bicer et al., *First Look at the Physics Case of TLEP*, *JHEP* **1401** (2014) 164, [arXiv:1308.6176].

[3] M. Ahmad et al., "CEPC-SPPC Preliminary Conceptual Design Report, Volume I: Physics and Detector." http://cepc.ihep.ac.cn/preCDR/volume.html, 2015.

[4] M. Baak, A. Blondel, A. Bodek, R. Caputo, T. Corbett, et al., *Working Group Report: Precision Study of Electroweak Interactions*, arXiv:1310.6708.

[5] J. Fan, M. Reece, and L.-T. Wang, *Possible Futures of Electroweak Precision: ILC, FCC-ee, and CEPC*, arXiv:1411.1054.

[6] J. Fan, M. Reece, and L.-T. Wang, *Precision Natural SUSY at CEPC, FCC-ee, and ILC*, arXiv:1412.3107.

[7] D. Curtin, R. Essig, S. Gori, and J. Shelton, *Illuminating Dark Photons with High-Energy Colliders*, *JHEP* **1502** (2015) 157, [arXiv:1412.0018].

[8] M. E. Peskin and T. Takeuchi, *Estimation of oblique electroweak corrections*, *Phys.Rev.* **D46** (1992) 381–409.

[9] R. Peccei, S. Peris, and X. Zhang, *Nonstandard couplings of the top quark and precision measurements of the electroweak theory*, *Nucl.Phys.* **B349** (1991) 305–322.

[10] K. Agashe, R. Contino, L. Da Rold, and A. Pomarol, *A Custodial symmetry for Zb anti-b*, *Phys.Lett.* **B641** (2006) 62–66, [hep-ph/0605341].

[11] H. E. Haber and H. E. Logan, *Radiative corrections to the Z b anti-b vertex and constraints on extended Higgs sectors*, *Phys.Rev.* **D62** (2000) 015011, [hep-ph/9909335].

[12] **ALEPH, DELPHI, L3, OPAL, SLD, LEP Electroweak Working Group, SLD Electroweak Group, SLD Heavy Flavour Group** Collaboration, S. Schael et al., *Precision electroweak measurements on the Z resonance*, *Phys.Rept.* **427** (2006) 257–454, [hep-ex/0509008].

[13] A. Freitas and Y.-C. Huang, *Electroweak two-loop corrections to $sin^2\theta^{b\bar{b}}_{eff}$ and R_b using numerical Mellin-Barnes integrals*, *JHEP* **1208** (2012) 050, [arXiv:1205.0299].

[14] **Gfitter Group** Collaboration, M. Baak et al., *The global electroweak fit at NNLO and prospects for the LHC and ILC*, *Eur.Phys.J.* **C74** (2014) 3046, [arXiv:1407.3792].

[15] A. Freitas, *Higher-order electroweak corrections to the partial widths and branching ratios of the Z boson*, *JHEP* **1404** (2014) 070, [arXiv:1401.2447].

[16] B. Batell, S. Gori, and L.-T. Wang, *Higgs Couplings and Precision Electroweak Data*, *JHEP* **1301** (2013) 139, [arXiv:1209.6382].

[17] M. Ciuchini, E. Franco, S. Mishima, and L. Silvestrini, *Electroweak Precision Observables, New Physics and the Nature of a 126 GeV Higgs Boson*, *JHEP* **1308** (2013) 106, [arXiv:1306.4644].

[18] H. Flacher, M. Goebel, J. Haller, A. Hocker, K. Monig, et al., *Revisiting the Global Electroweak Fit of the Standard Model and Beyond with Gfitter*, *Eur.Phys.J.* **C60** (2009) 543–583, [arXiv:0811.0009].

[19] A. Pomarol and F. Riva, *Towards the Ultimate SM Fit to Close in on Higgs Physics*, *JHEP* **01** (2014) 151, [arXiv:1308.2803].

[20] J. Ellis, V. Sanz, and T. You, *The Effective Standard Model after LHC Run I*, *JHEP* **03** (2015) 157, [arXiv:1410.7703].

[21] A. Falkowski and F. Riva, *Model-independent precision constraints on dimension-6 operators*, *JHEP* **02** (2015) 039, [arXiv:1411.0669].

[22] L. Berthier and M. Trott, *Towards consistent Electroweak Precision Data constraints in the SMEFT*, *JHEP* **05** (2015) 024, [arXiv:1502.02570].

[23] L. Berthier and M. Trott, *Consistent constraints on the Standard Model Effective Field Theory*, arXiv:1508.05060.

[24] **Particle Data Group** Collaboration, K. Olive et al., *Review of Particle Physics*, *Chin.Phys.* **C38** (2014) 090001.

[25] **ATLAS, CDF, CMS, D0** Collaboration, *First combination of Tevatron and LHC measurements of the top-quark mass*, arXiv:1403.4427.

[26] **ATLAS** Collaboration, G. Aad et al., *Measurement of the Higgs boson mass from the $H \to \gamma\gamma$ and $H \to ZZ^* \to 4\ell$ channels with the ATLAS detector using 25 fb^{-1} of pp collision data*, *Phys.Rev.* **D90** (2014), no. 5 052004, [arXiv:1406.3827].

[27] **CMS** Collaboration, *Precise determination of the mass of the Higgs boson and studies of the compatibility of its couplings with the standard model*, CMS-PAS-HIG-14-009.

[28] M. Davier, A. Hoecker, B. Malaescu, and Z. Zhang, *Reevaluation of the Hadronic Contributions to the Muon g-2 and to alpha(MZ)*, *Eur.Phys.J.* **C71** (2011) 1515, [arXiv:1010.4180].

[29] C. W. Murphy, *Bottom-Quark Forward-Backward and Charge Asymmetries at Hadron Colliders*, arXiv:1504.02493.

[30] A. Pich, *Review of α_s determinations*, *PoS* **ConfinementX** (2012) 022, [arXiv:1303.2262].

[31] M. Ciuchini, E. Franco, S. Mishima, M. Pierini, L. Reina, et al., *Update of the electroweak precision fit, interplay with Higgs-boson signal strengths and model-independent constraints on new physics*, arXiv:1410.6940.

[32] D. Choudhury, T. M. Tait, and C. Wagner, *Beautiful mirrors and precision electroweak data*, *Phys.Rev.* **D65** (2002) 053002, [hep-ph/0109097].

[33] **ATLAS** Collaboration, G. Aad et al., *Search for charged Higgs bosons decaying via $H^\pm \to \tau^\pm\nu$ in fully hadronic final states using pp collision data at $\sqrt{s} = 8$ TeV with the ATLAS detector*, *JHEP* **1503** (2015) 088, [arXiv:1412.6663].

[34] **CMS** Collaboration, *Search for a heavy charged Higgs boson in proton-proton collisions at sqrts=8 TeV with the CMS detector*, CMS-PAS-HIG-13-026.

[35] N. Craig, F. DEramo, P. Draper, S. Thomas, and H. Zhang, *The Hunt for the Rest of the Higgs Bosons*, *JHEP* **1506** (2015) 137, [arXiv:1504.04630].

[36] L. Da Rold, *Solving the A^b_{FB} anomaly in natural composite models*, *JHEP* **1102** (2011) 034, [arXiv:1009.2392].

[37] C. Grojean, O. Matsedonskyi, and G. Panico, *Light top partners and precision physics*, *JHEP* **1310** (2013) 160, [arXiv:1306.4655].

[38] G. Panico and A. Wulzer, *The Composite Nambu-Goldstone Higgs*, arXiv:1506.01961.

[39] O. Matsedonskyi, G. Panico, and A. Wulzer, *Light Top Partners for a Light Composite Higgs*, *JHEP* **01** (2013) 164, [arXiv:1204.6333].

[40] A. Thamm, R. Torre, and A. Wulzer, *Future tests of Higgs compositeness: direct vs indirect*, arXiv:1502.01701.

[41] D. Barducci, S. De Curtis, S. Moretti, and G. M. Pruna, *Top pair production at a future e^+e^- machine in a composite Higgs scenario*, arXiv:1504.05407.

[42] J. Aguilar-Saavedra, R. Benbrik, S. Heinemeyer, and M. Prez-Victoria, *Handbook of vectorlike quarks: Mixing and single production*, *Phys.Rev.* **D88** (2013), no. 9 094010, [arXiv:1306.0572].

[43] D. E. Morrissey and C. E. M. Wagner, *Beautiful mirrors, unification of couplings and collider phenomenology*, *Phys. Rev.* **D69** (2004) 053001, [hep-ph/0308001].

[44] K. Kumar, W. Shepherd, T. M. Tait, and R. Vega-Morales, *Beautiful Mirrors at the LHC*, *JHEP* **1008** (2010) 052, [arXiv:1004.4895].

[45] **CMS** Collaboration, *Search for vector-like quarks in final states with a single lepton and jets in pp collisions at sqrt s = 8 TeV*, CMS-PAS-B2G-12-017.

[46] **CMS** Collaboration, *Search for pair-produced vector-like quarks of charge -1/3 decaying to bH using boosted Higgs jet-tagging in pp collisions at sqrt(s) = 8 TeV*, CMS-PAS-B2G-14-001.

[47] E. lvarez, L. Da Rold, and J. I. Sanchez Vietto, *Single production of an exotic bottom partner at LHC*, *JHEP* **1402** (2014) 010, [arXiv:1311.2077].

[48] G. Salam and A. Weiler, "Collider Reach (β)." http://collider-reach.web.cern.ch/collider-reach/.

[49] R. Dermisek, S.-G. Kim, and A. Raval, *New Vector Boson Near the Z-pole and the Puzzle in Precision Electroweak Data*, *Phys.Rev.* **D84** (2011) 035006, [arXiv:1105.0773].

[50] R. Dermisek, S.-G. Kim, and A. Raval, *Z' near the Z-pole*, *Phys.Rev.* **D85** (2012) 075022, [arXiv:1201.0315].

[51] M. Awramik, M. Czakon, A. Freitas, and B. A. Kniehl, *Two-loop electroweak fermionic corrections to* $\sin^2\theta^{b\bar{b}}_{\rm eff}$, *Nucl. Phys.* **B813** (2009) 174–187, [arXiv:0811.1364].